



## ORIGINAL ARTICLE

# Eco-friendly synthesis of size-controlled silver nanoparticles by using *Areca catechu* nut aqueous extract and investigation of their potent antioxidant and anti-bacterial activities



Xiaoping Hu<sup>a,b,1</sup>, Lingfeng Wu<sup>a,1</sup>, Minjie Du<sup>a</sup>, Lu Wang<sup>a,b,\*</sup>

<sup>a</sup> School of Food Science and Engineering, Hainan University, Haikou 570228, PR China

<sup>b</sup> Key Laboratory of Food Nutrition and Functional Food of Hainan Province, Hainan University, Haikou 570228, PR China

Received 25 September 2021; accepted 1 February 2022

Available online 11 February 2022

## KEYWORDS

*Areca catechu* L. nut;  
Eco-friendly synthesis;  
Silver nanoparticles;  
Antioxidant activities;  
Anti-bacterial activities

**Abstract** Silver nanoparticles (AgNPs) have attracted considerable attention owing to their unique biological applications. AgNPs synthesized by plant extract is considered as a convenient, efficient and eco-friendly material. In this work, the aqueous extract of *Areca catechu* L. nut (ACN) was used as the reducing and capping agents for one-pot synthesis of AgNPs, and their antioxidant and antibacterial activities were investigated. UV (Ultra Violet)-visible spectrum and dynamic light scattering (DLS) analysis revealed that the size of AgNPs was sensitive to the synthesis conditions. The synthesized AgNPs were composed of well-dispersed particles with an small size of about 10 nm under the optimal conditions (pH value of extract was 12.0; AgNO<sub>3</sub> concentration was 1.0 mM; reaction time was 90 min). In addition, scanning electron microscope with energy dispersive X-ray (SEM-EDX), transmission electron microscopy (TEM) and X-ray diffraction (XRD) results further verified that the synthesized AgNPs had a stable and well-dispersed form (Zeta potential value of -30.50 mV and polydispersity index of 0.328) and a regular spherical shape (average size of 15–20 nm). In addition, Fourier transform infrared spectrometry (FTIR) results revealed that phytochemical constituents in ACN aqueous extract accounted for Ag<sup>+</sup> ion reduction, capping and stabilization of AgNPs. The possible reductants in the aqueous extract of *Areca catechu* L. nut were identified by high-performance liquid chromatography-electrospray ionization-quadrupole-time of flight-mass spectrometry (HPLC-ESI-qTOF/MS) method. More importantly, the synthesized AgNPs indicated excellent free radical scavenging activity of 1,1-diphenyl-2-

\* Corresponding authors at: School of Food Science and Engineering, Hainan University, Haikou 570228, PR China.

E-mail address: [lwang@hainanu.edu.cn](mailto:lwang@hainanu.edu.cn) (L. Wang).

<sup>1</sup> These authors contributed equally to this work.

Peer review under responsibility of King Saud University.



picrylhydrazyl (DPPH<sup>•</sup>; IC<sub>50</sub> = 11.75 ± 0.29 µg/mL) and 2,2-azino-bis (3-ethylbenzothiazoline-6-sulfonic acid) diammonium salt (ABTS<sup>+</sup>; IC<sub>50</sub> = 44.85 ± 0.37 µg/mL), which were significant higher than that of ascorbic acid. Moreover, AgNPs exhibited an enhanced antibacterial activity against six selected common pathogens (especially *Escherichia coli* and *Staphylococcus aureus*) compared with AgNO<sub>3</sub> solution. In a short, this study showed that the *Areca catechu* L. nut aqueous extract could be applied for eco-friendly synthesis of AgNPs.

© 2022 The Author(s). Published by Elsevier B.V. on behalf of King Saud University. This is an open access article under the CC BY license (<http://creativecommons.org/licenses/by/4.0/>).

## 1. Introduction

As a fast developing and challenging technology, nanotechnology has been well applied in bio-medical engineering and pharmaceutical industry (Kanagamani et al., 2019; Momeni et al., 2017). Compared with bulk materials, nanoparticles have advantages of large surface-area-to-volume ratio, excellent optical and electrical conductivity, and ideal catalytic properties (Mani et al., 2021a, 2021b; Rasheed et al., 2020; Sher et al., 2020). Silver nanoparticles (AgNPs) have attracted considerable attention owing to its potential application value in many aspects such as catalysis, biosensors, electronics, adsorptive remediation of hazardous environmental pollutants, and biomedicine engineering (Ameen et al., 2021; Prema et al., 2022; Rasheed et al., 2020). Consequently, it is necessary to develop a simple, mild, and eco-friendly synthesis path of AgNPs. Generally, electrochemical techniques, physical radiation, and chemical reduction are common methods for the synthesis of AgNPs (Beyene et al., 2017; Lee and Jun 2019). However, most of these methods involve the usage of various hazardous and toxic chemicals, organic solvents, high temperatures, and environmentally harmful procedures (Iravani, 2011; Mani et al., 2021c). Currently, synthesis methods have been proven to be non-toxic and eco-friendly strategies for large-scale production. Normally, microorganisms, bio-macromolecules and plant extracts can be considered as the eco-friendly reducing agents for the synthesis of metal nanoparticles (Lotfollahzadeh et al., 2021). Compared with microorganisms or bio-macromolecules, plant extracts have the advantage of easy accessibility, less bio-threat and higher content of reductants. Currently, various plant extracts have been widely applied to the synthesis of NPs (Begic et al., 2021; Yulizar et al., 2020).

To date, various plants extracts have been applied to the preparation of different sized and shaped NPs with potential *in vivo* biological activities (Hajipour et al., 2012; Yulizar et al., 2020). Venkatadri et al. (2020) synthesized AgNPs using aqueous rhizome extract of *Zingiber officinale* and *Curcuma longa*, and found the synthesized AgNPs had strong anti-bacterial activities. Wei et al. (2020) successfully synthesized size-controlled AgNPs by using the *Sea buckthorn* berry extract, and found the prepared AgNPs had significant antioxidant and antibacterial activity. *Areca catechu* L. belongs to *Areaceae* family, which is widely planted in China, Indonesia, Malaysia, and India, etc. *Areca catechu* L. is also considered as a herbal medicine listed in the Chinese Pharmacopoeia (Sazwi et al., 2013). Extensive investigations have verified that the extract of *Areca catechu* L. nut (ACN) comprises many bio-active compounds, such as phenolics, flavonoids, and polysaccharide, etc. These compounds not only have multiple pharmacological activities, such as antimicrobial, antioxidant, anti-osteoporosis, anti-inflammatory, and anti-parasitic effects, etc., but also can be used as the reductants in the synthesis of AgNPs (Bhat et al., 2012; Rajan et al., 2015; Shen et al., 2017). Many researchers have verified that the size and distribution of AgNPs are largely determined by the reductant molecules from plant extracts (Rajan et al., 2015; Wei et al., 2021). The strong reductant molecules in the extract lead to the formation of smaller nanoparticles (Rajan et al., 2015; Wei et al., 2021). Although the biological activity of AgNPs synthesized using plant extracts have been reported, there is a lack of studies on the synthesis of AgNPs using areca nut (*Areca catechu*) extract.

In this study, a simple and eco-friendly synthesis method of AgNPs by using the ACN aqueous extract was developed. Importantly, the effects of synthesis parameters, such as the concentration of AgNO<sub>3</sub>, pH value of the extract and reaction time on as-prepared AgNPs were for the first time. Then, the as-synthesized AgNPs were further characterized by UV-visible spectrum, SEM-EDX, TEM, XRD, FTIR, and Zeta potential analysis. The possible reductants in the aqueous extract of ACN were also identified by HPLC-ESI-qTOF/MS method for the first time. Additionally, multi-biological properties of the synthesized AgNPs were systematically evaluated. These findings reveal that the AgNPs synthesized by using the ACN extract could be used as a potent antioxidant and antibacterial agent in environmental protection.

## 2. Materials and methods

### 2.1. Materials and chemicals

Fresh reference specimens *Areca catechu* L. were collected from Hainan (Chengmai village, Hainan, China-19° 32' 39" N, 111° 7' 21" E) in December 20th, 2019. The samples specimens (201912WL) were identified by Professor Weimin Zhang (College of Food Science and Engineering, Hainan University, Haikou, Hainan, China). All phenolic standards (HPLC-grade, > 99.8%) and ascorbic acid (Vc, ≥ 99.8%) were purchased from Sigma-Aldrich Co., Ltd. (Shanghai, China). Silver nitrate (AgNO<sub>3</sub>, > 99.7%), 2,2-azino-bis (3-ethylbenzothiazoline-6-sulfonic acid) diammonium salt (ABTS, > 99.7%), and 1,1-diphenyl-2-picrylhydrazyl (DPPH<sup>•</sup>, > 99.8%) were purchased from Aladdin Reagent Co., Ltd. (Shanghai, China). Acetonitrile and formic acid of chromatographic-grade were purchased from Macklin Reagent Co., Ltd. (Shanghai, China). Ultra-pure deionized water was prepared by a Millipore Milli-Q water purification system (Bedford, Massachusetts, USA). Common food pathogen bacteria were supplied by Guangdong Microbial Culture Collection Center (Guangdong, China). Gram positive bacteria included *Listeria monocytogenes* (ATCC 51772), *Staphylococcus aureus* (ATCC 25923), and *Bacillus subtilis* (ATCC 14579). Gram negative bacteria included *Escherichia coli* (ATCC 25922), *Salmonella typhimurium* (ATCC 14028), and *Pseudomonas aeruginosa* (ATCC 27853).

### 2.2. Extraction and identification of chemical components from ACN

Firstly, the seed of *Areca catechu* L. was removed. The *Areca catechu* L. nut (ACN) was washed thoroughly with sterile deionized water, freeze-dried and powdered by a JGY 2500B type micro-mill (Jinhua, Zhejiang). Then, the ACN powder (5 g) was mixed with 100 mL of sterile deionized water, and heated at 50 °C for 30 min under vigorous shaking. Subsequently, the extracts were centrifuged at 10,000g for 10 min

before collecting and storing the supernatant at 4 °C for the subsequent assays.

The chemical components in the ACN aqueous extracts were identified by using an Agilent 1260 HPLC-DAD system equipped with an Bruker microTOF-Q II mass detector (Li et al., 2022; Wang et al., 2022). 10 µL of the extract was separated by an temperature-controlled Zorbax SB C<sub>18</sub> plus column (Aligent, 250 mm × 4.6 mm, 3.5 µm, CA, USA) at 30 °C. The gradient elution of solvent A (acetonitrile) and solvent B (0.1% formic acid-water) was conducted as follow: 0–6 min, 15% solvent A; 6–20 min, 15–25% solvent A; 20–40 min, 25–50% solvent A; 40–45 min, 80% solvent A. UV-vis DAD wavelength detection was conducted within the range from 200 to 600 nm. Chemical components in the ACN extracts were determined by analyzing their MS fragmentation, comparing retention times with the standards in HPLC chromatograms and referring to the previous references (Shen et al., 2017; Wang et al., 2021).

### 2.3. Synthesis of AgNPs

The schematic diagram describing the synthesis of the AgNPs using the aqueous extract of *Areca catechu* nut is shown in Fig. 1. The synthesis of AgNPs was carried out by mixing 50 mL of 1 mg/mL ACN aqueous extracts with 50 mL of AgNO<sub>3</sub> solution. The influences of synthesis parameters

including the concentration of AgNO<sub>3</sub> solution (0, 0.1, 0.2, 0.4, 0.6, 0.8, and 1.0 mM), the pH value of the extract (pH = 2.0, 4.0, 6.0, 8.0, 10.0, and 12.0) and the reaction time (5, 10, 30, 60, 90, and 120 min) were investigated. The color of mixed solution turned to dark orange, indicating successful synthesis of AgNPs (Begic et al., 2021; Lotfollahzadeh et al., 2021). The reduction process of silver ions was analyzed by using a UV-2802SH spectrophotometer (Shanghai, China) within the range from 300 to 700 nm (Begic et al., 2021; Lotfollahzadeh et al., 2021). Zetasizer Nano Instrument (Malvern, Britain) was used to measure the particle size of the above AgNPs colloidal solution. Under the optimal conditions, the mixture was centrifuged at 4000g for 20 min before obtaining the purified AgNPs. The obtained precipitates were washed three times using deionized water and then lyophilized for 24 h for subsequent characterization.

### 2.4. Characterization of the purified AgNPs

The morphology of the synthesized AgNPs under optimal conditions was observed by using scanning electron microscope equipped with energy dispersive X-ray (SEM-EDX) and transmission electron microscopy (TEM) (JEM-2010, Tokyo, Japan) (Wei et al., 2021)). The particle size and stability of the prepared AgNPs colloidal solution were determined using a Zetasizer Nano Instrument (Malvern Instruments Ltd., Mal-

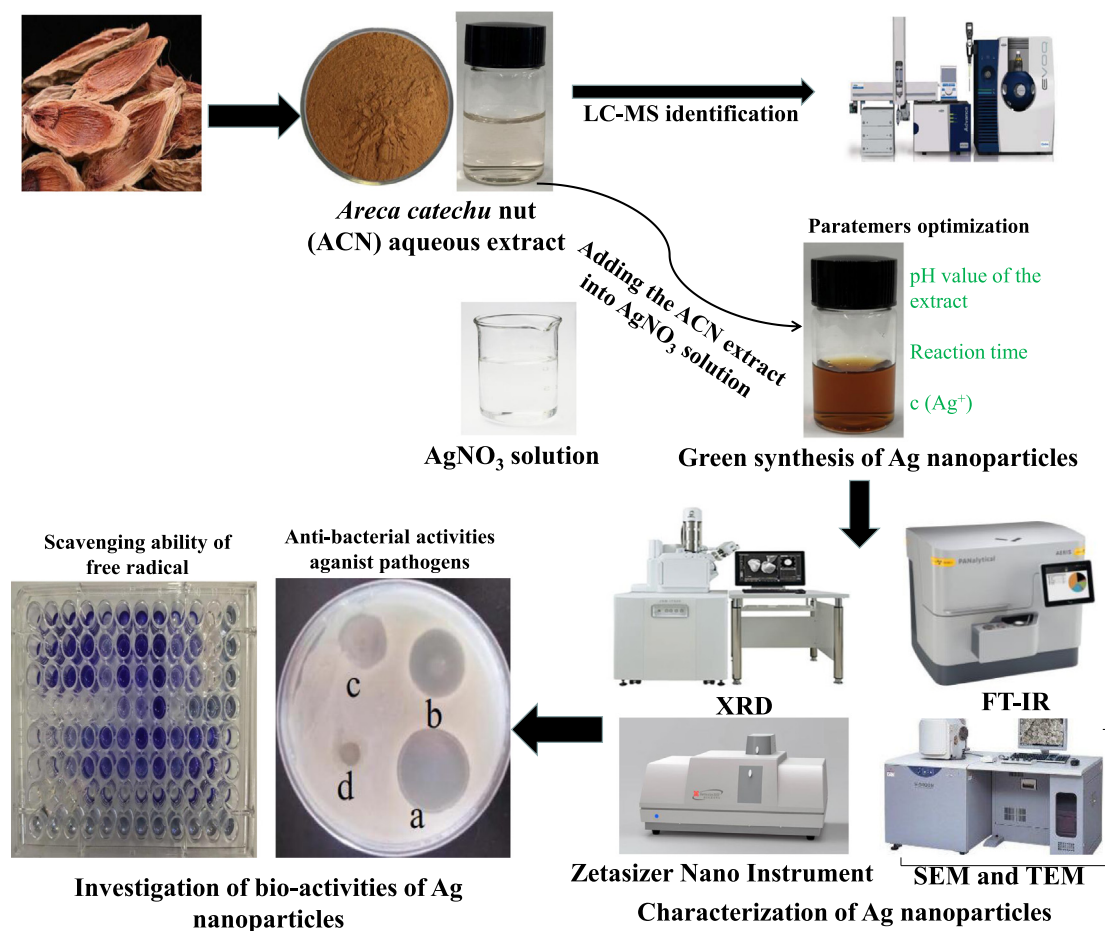


Fig. 1 Schematic diagram describing the synthesis of the silver nanoparticles using the aqueous extract of *Areca catechu* nut.

vern, UK) (Wei et al., 2021). In order to determine the functional groups of biomolecules in the plant extract, Fourier transform infrared spectrometry (FTIR) was used for purified AgNPs within the range of 400–4000  $\text{cm}^{-1}$  (PerkinElmer Spotlight 400 FTIR, MA, USA) (Wang et al., 2018a,b). X-ray diffraction (XRD) analysis was carried out to evaluate the crystalline phase of the synthesized AgNPs by using SHIMADZU XRD6000 (Shimadzu, Japan). The XRD patterns were recorded at  $2\theta$  angles from  $20^\circ$  to  $80^\circ$ . The average crystallite size ( $D$ , nm) of the AgNPs was calculated by using the Debye-Scherrer equation as described in Eq. (1) (Gur et al., 2022):

$$D = \frac{k\lambda}{\alpha \cos\theta} \quad (1)$$

where  $D$  denotes crystallite size,  $k$  represents the shape factor,  $\lambda$  is the wavelength of the XRD,  $\theta$  is the angle of diffraction, and  $\alpha$  is the half-width of the peak.

### 2.5. Anti-oxidant activity assay

An DPPH $^{\cdot}$  assay was performed based on the method reported by Wu et al. (2020). Briefly, 50  $\mu\text{L}$  of AgNPs (5, 10, 20, 50, 100, and 150  $\mu\text{g}/\text{mL}$ ) were added to 400  $\mu\text{L}$  of 100  $\mu\text{M}$  DPPH-methanol solution, and then kept in the dark at  $25^\circ\text{C}$  for 30 min before recording the absorbance at 517 nm. An ABTS $^{+\cdot}$  assay was conducted according to the method described in Zhu et al. (2020). To be specific, the ABTS $^{+\cdot}$  working solution was prepared by diluting the fresh ABTS $^{+\cdot}$  stock solution (7 mM ABTS $^{+\cdot}$  and 2.45 mM  $\text{K}_2\text{S}_2\text{O}_8$  at the volume ratio 1:1) within an absorbance of 0.70 at 734 nm. 50  $\mu\text{L}$  of AgNPs (5, 10, 20, 50, 100, and 150  $\mu\text{g}/\text{mL}$ ) were well mixed with 400  $\mu\text{L}$  of the above diluted ABTS $^{+\cdot}$  working solution, and then incubated in the dark for 30 min at  $25^\circ\text{C}$  before recording the absorbance at 734 nm. The ultrapure water was used as the negative control. The radical scavenging ability of DPPH $^{\cdot}$ /ABTS $^{+\cdot}$  was determined by Eq. (2):

Free radical scavenging ability(%)

$$= \frac{A_{\text{blank}} - A_{\text{sample}}}{A_{\text{blank}}} \times 100 \quad (2)$$

where  $A_{\text{blank}}$  is the absorbance of ultra-pure water and DPPH $^{\cdot}$ /ABTS $^{+\cdot}$  solution;  $A_{\text{sample}}$  is the absorbance of the AgNPs and DPPH $^{\cdot}$ /ABTS $^{+\cdot}$  solution.

### 2.6. Anti-bacterial activity assay

Anti-bacterial activity of the synthesized AgNPs was measured according to the standard two-fold serial dilution method described by Jorgensen, (1993). The minimum inhibitory concentration (MIC) and minimum bactericidal concentration (MBC) against the tested bacterial strains were determined by standardized agar dilution method. Briefly, all the tested foodborne pathogens were cultured on Luria-Bertani liquid medium to obtain a concentration of  $1 \times 10^6$  CFU/mL. Then, a serial dilutions of the synthesized AgNPs (0.1–1000  $\mu\text{g}/\text{mL}$ ),  $\text{AgNO}_3$  solution (0.1–1000  $\mu\text{g}/\text{mL}$ ), and the ACN extracts (0.1–2048  $\mu\text{g}/\text{mL}$ ) were prepared. Subsequently, 100  $\mu\text{L}$  of the serial dilutions of AgNPs or the ACN extracts and 100  $\mu\text{L}$  of the above inoculum suspension ( $1 \times 10^6$  CFU/mL) were well mixed in a 96-microwell plate

and incubated at  $35^\circ\text{C}$  for 30 h. Finally, the absorbance at 600 nm was recorded using a UV-2802SH type spectrophotometer (Shanghai, China). Tetracycline hydrochloride (0.1–10  $\mu\text{g}/\text{mL}$ ) was used as the positive control. All the tests were performed in triplicate.

### 2.7. Statistical analysis

Statistical analysis was carried out by one-way analysis of variance analysis (ANOVA) in IBM SPSS version 23.0 software (IBM Corp., Armonk, NY, USA). The difference was considered statistically significant when  $p < 0.05$ . All data were expressed in the form of mean  $\pm$  standard deviation based on three independent replicates.

## 3. Results and discussion

### 3.1. Effects of synthesis parameters on the synthesized AgNPs

In general, the formation and stability of metal nanoparticles in the reaction mixture can be detected by UV-Vis absorption spectroscopy methods (Begic et al., 2021; Lotfollahzadeh et al., 2021). The absorbance of the ACN aqueous extract and  $\text{AgNO}_3$  solution above 420 nm was negligible. The UV-vis spectra of AgNPs synthesized showed a surface plasmon resonance peak (SPRP) at about 420 nm due to the generation of AgNPs (Aygün et al., 2020; Wei et al., 2020). It is worth noting that a SPRP at about 520 nm indicated the generation of  $\text{Ag}_2\text{O}$  NPs (Sathishkumar et al., 2009; Verma and Mehata, 2020). This study established that the synthesis of NPs using ACN extract extracted by ultra-pure deionized water did not result in the formation of  $\text{Ag}_2\text{O}$  NPs. It has been reported that the concentration of the extracts or  $\text{AgNO}_3$  solution, pH value, temperature and incubation time are key parameters affecting the particle size and shape of the synthesized nanoparticles (Wei et al., 2020; Wei et al., 2021). In this work, the synthesis conditions of AgNPs were investigated. Initially, a rapid reaction was observed when mixing 50 mL of 1 mg/mL ACN aqueous extract with the  $\text{AgNO}_3$  solution at ambient temperature. It was observed that the color of the reaction mixture gradually turned from light yellow to dark orange as the concentration of  $\text{AgNO}_3$  solution increased, indicating the formation of AgNPs (Fig. 2A). According to the UV-Vis spectra measurement, the synthesized AgNPs exhibited a surface plasmon resonance peak around 415 nm. Moreover, the maximum absorbance peak at 415 nm was strengthened as the concentration of  $\text{AgNO}_3$  solution increased (Fig. 2B). To further characterize the spectral evolution, the average size of the as-prepared AgNPs colloidal solution under different  $\text{AgNO}_3$  concentrations was measured using DLS technique. As shown in Fig. 2C, with the increase of  $\text{AgNO}_3$  concentration, the average size of as-synthesized AgNPs decreased from  $119.2 \pm 2.0$  nm to  $8.98 \pm 0.28$  nm, indicating that a high concentration of  $\text{AgNO}_3$  solution may be more beneficial for obtaining the smaller-sized AgNPs particles (Wei et al., 2020). Ahmad et al. (2021) successfully synthesized AgNPs by using *Flacourtia jangomas* fruit extract and 1.0 mM  $\text{AgNO}_3$  solution, and found the AgNPs were in a regular spherical shape with the average crystallite size of 8.29 nm. Hence, 1.0 mM  $\text{AgNO}_3$  solution was more conducive for the synthesis of smaller-sized AgNPs.

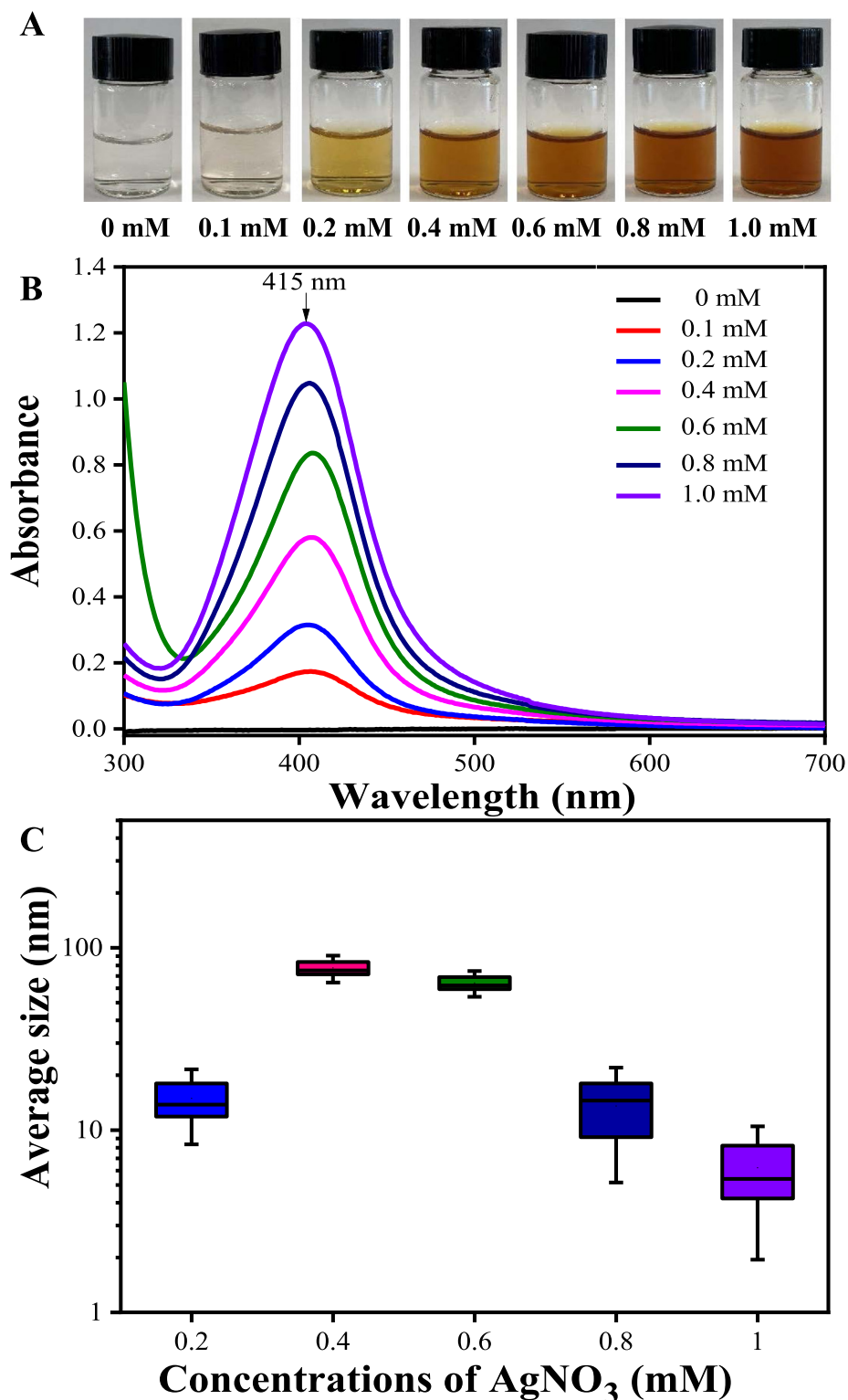


**Fig. 2** The color (A), UV-vis spectra (B) and the average size (C) changes of the bio-reduction kinetics of a colloidal AgNPs solution synthesized by the ACN aqueous extracts (1 mg/mL) and  $\text{AgNO}_3$  at different concentrations at pH = 10.0, 25 °C for 90 min.

Wei et al. (2020) reported that pH value of the extracts was an important parameter influencing the average size of the prepared AgNPs. Under fixing concentration of  $\text{AgNO}_3$  (1.0 mM), the color of the mixture solution gradually turned to dark orange as the pH value of the extract increased

(Fig. 3A). As shown in Fig. 3AB, when the pH value of the extract increased from 2 to 12, the yield of synthesized AgNPs evidently increased. Moreover, the maximum absorbance peak shifted from 430 nm to 412 nm with the increase of pH value of the extract, indicating that smaller-sized AgNPs were gener-

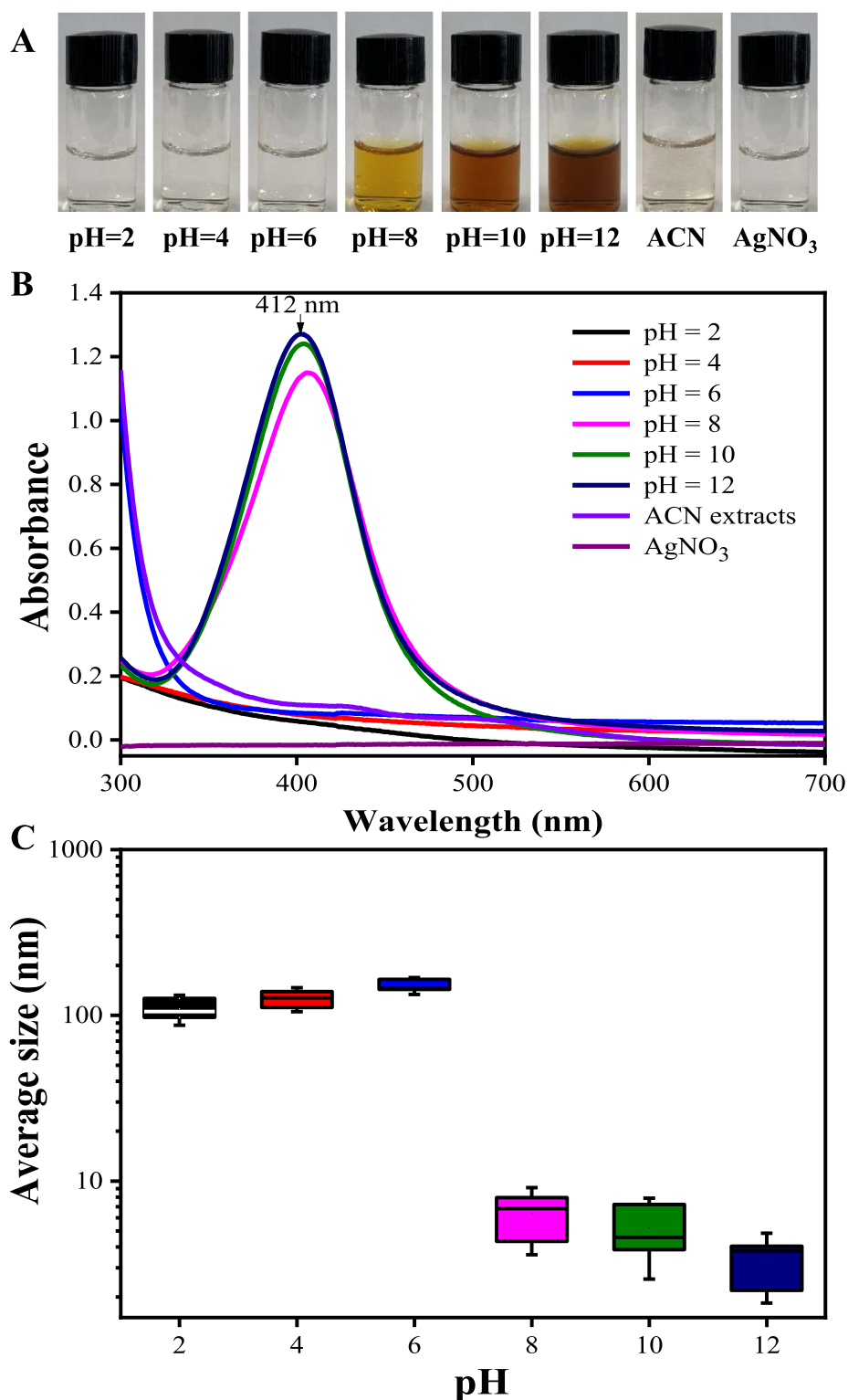


**Fig. 3** The color (A), UV-vis spectra (B) and the average size (C) changes of the bio-reduction kinetics of a colloidal AgNPs solution synthesized by the ACN aqueous extracts (1 mg/mL) and AgNO<sub>3</sub> (1.0 mM) under different pH values at 25 °C for 90 min.

ated at a high pH value. Researchers have verified that the shift of nucleation and growth kinetics at a high pH condition may improve the bio-availability of functional groups, thereby enhancing the formation of smaller sized AgNPs (Verma and Mehata, 2020). As shown in Fig. 3C, with the increase of pH

value of the extract, the average size of prepared AgNPs evidently decreased from  $102.98 \pm 5.01$  nm to  $10.25 \pm 1.69$  nm, showing the quicker nucleation rate under high pH condition, which was consistent with the results reported by Sathishkumar et al. (2009). In this work, the result of DLS

analysis showed that the synthesized AgNPs with small size (< 10 nm) was obtained under alkaline condition (pH = 12), which was consistent with the result of [Ebrahimzadeha et al. \(2020\)](#) who reported the fabricated AgNPs at alkaline pH had a smaller average size compared with the AgNPs synthesized under acidic condition.

After mixing 50 mL of 1 mg/mL the ACN extract with 50 mL of 1.0 mM AgNO<sub>3</sub> solution at pH = 12.0, the color-shift and UV-vis spectra of reaction mixture were recorded at intervals ([Fig. 4AB](#)). A position-shift from 425 to 408 nm showed that the as-prepared smaller-sized AgNPs were formed after reaction for 90 min. [Wei et al. \(2020\)](#) verified that the average size of the AgNPs prepared by the berry extract of *Sea Buckthorn* decreased with the extending of reaction time. Moreover, the DLS measurements confirmed that the average size of as-prepared AgNPs continuously decreased with the reaction time ([Fig. 4C](#)). In order to yield more smaller-sized AgNPs products, AgNPs were synthesized by mixing 50.0 mL of the ACN aqueous extract (pH = 12) with 50.0 mL of 1.0 mM AgNO<sub>3</sub> solution and then keeping the reaction for 90 min.

### 3.2. Characterization of the synthesized AgNPs

[Fig. 5A](#) shows the SEM image of the synthesized AgNPs under the extract pH value of 12.0, 1.0 mM of AgNO<sub>3</sub> concentration of 1.0 mM, and the reaction time of 90 min. It can be observed that the prepared AgNPs were in a regular quasi-spherical shape with the average size of about 15–20 nm. A small amount of larger sized AgNPs was formed because of the agglomeration of particles induced by freeze drying. The elemental profiles of the purified AgNPs were investigated by SEM equipped with an EDX detector ([Fig. 5B](#)). The result showed that a high signal peak of Ag (2.5–3.5 keV) existed in the fabricated AgNPs, followed by signal peaks of C and O elements. The insert table in [Fig. 5B](#) lists the atomic percent in the prepared AgNPs. The C and O elements identified may come from phytochemical components, which were bonded to the surfaces of the AgNPs. As can be seen in [Fig. 5C](#), the results of the TEM analysis are in agreement with results of the SEM analysis. The AgNPs were in regular spherical shape with a smaller average size of  $16.51 \pm 2.1$  nm. The insert table in [Fig. 5D](#) shows the prepared AgNPs had a high Zeta potential value (–30.50 mV) and a low poly-dispersity index of 0.328, indicating the high stability and excellent dispersion. [Kuznetsova and Rempela](#) reported that the synthesized nanoparticles with Zeta potential value < –25 mV or > +25 mV had a high degree of stability ([Kuznetsova and Rempela, 2015](#)). In addition, the capping agents with negative charge groups were attached to the surface of nanoparticles, resulting in a negative Zeta potential value of AgNPs ([Sathishkumar et al., 2009](#); [Verma and Mehata, 2020](#); [Wei et al., 2020](#)). The repulsive force between the negative charged nanoparticles prevented widespread agglomeration of colloidal AgNPs solution.

As shown in [Fig. 6A](#), six prominent diffraction peaks were found in XRD patterns at  $2\theta$  values of 28.03°, 32.35°, 38.31°, 46.87°, 65.29°, and 76.81°, which respectively corresponded to (210), (122), (111), (200), (220), and (311) Bragg's reflections of the face-centered cubic (FCC) structure of silver from the Joint Committee of Powder Diffraction Standard (No.

087-0720). The average crystal size of the synthesized AgNPs was calculated according to Eq. (1), which was  $17.89 \pm 0.96$  nm.

The FTIR spectra of the ACN extract and the prepared AgNPs are shown in [Fig. 6B](#). The characteristic peaks around 3419 cm<sup>-1</sup> were ascribed to the O–H stretching vibration of OH– structure groups. The peak around 2932 cm<sup>-1</sup> was ascribed to C–H stretching vibration. The sharp peak at 1603 cm<sup>-1</sup> was ascribed to C=C stretching vibration of aromatic rings. The characteristic peaks around 1442 cm<sup>-1</sup> and 1475 cm<sup>-1</sup> were assigned to heterocyclic vibration (polyphenols). Additionally, the characteristic peaks around 1063 cm<sup>-1</sup> and 688 cm<sup>-1</sup> were attributed to alkyne C–H bending vibration. It can be observed that the intensity of peaks around 1603 cm<sup>-1</sup> and 1063 cm<sup>-1</sup> in the prepared AgNPs was weakened, indicating the involvement of the functional groups in the process of the reducing Ag<sup>+</sup> into Ag<sup>0</sup>. The FTIR results verified that the bio-active molecules in the ACN aqueous extract were distributed on the surfaces of AgNPs and responsible for the reduction of silver ions, which is in consistency with the previous reported results ([Yuvakkumar et al., 2014](#)).

### 3.3. Identification of possible reductants in *Areca catechu L. nut* aqueous extract

Many researchers have confirmed that secondary metabolites from plant extracts play important roles in the synthesis of AgNPs ([Wang et al., 2018a,b](#)). In this study, thirteen phenolic compounds in the ACN aqueous extract were identified by HPLC-ESI-qTOF-MS/MS method ([Wang et al., 2021](#)). From [Fig. 7](#) and [Table 1](#), compound 1 showing the parent ion at  $m/z$  of 171.02 [M + H]<sup>+</sup> was verified as gallic acid. Compounds 2 and 3 with the same parent ions  $m/z$  of 307.08 [M + H]<sup>+</sup> were identified as two catechin derivatives isomers. Through comparing with the retention time of the standards, compounds 2 and 3 were determined as (–)-gallocatechin and epigallocatechin, respectively. Presenting [M + H]<sup>+</sup> ion at  $m/z$  291.07, compound 4 was easily determined as d-catechin. Compound 6 showed the parent fragment ion at 193.05 [C<sub>10</sub>H<sub>10</sub>O<sub>4</sub>-H]<sup>-</sup>, which was easily identified as ferulic acid by comparison of mass spectrometry, standard and the database ([Lin et al., 2021](#)). Compound 7 showing quasimolecular [M–H]<sup>-</sup> ion at 609.15 and two MS/MS characteristic fragment ions at  $m/z$  449.10 [C<sub>27</sub>H<sub>30</sub>O<sub>16</sub>-Glc + H]<sup>+</sup> (lost of glucoside) and 303.05 [C<sub>15</sub>H<sub>10</sub>O<sub>7</sub> + H]<sup>+</sup> was easily identified as rutin. Peak 8, with the quasimolecular ion [C<sub>27</sub>H<sub>30</sub>O<sub>15</sub>-H]<sup>-</sup> at 593.16, and the MS/MS characteristic fragment ions at  $m/z$  433.2113 [C<sub>27</sub>H<sub>30</sub>O<sub>15</sub>-Gal + H]<sup>+</sup> (lost of galactoside), 303.16 [C<sub>15</sub>H<sub>10</sub>O<sub>7</sub> + H]<sup>+</sup> and 153.0302 [Gal + H]<sup>+</sup>, was tentatively determined as quercetin-3-*O*-galactoside ([Wang et al., 2021](#)). Presenting parent ion at 449.11 [C<sub>21</sub>H<sub>20</sub>O<sub>11</sub>-H]<sup>-</sup> and two fragment ions at  $m/z$  287.0609 [C<sub>15</sub>H<sub>10</sub>O<sub>6</sub> + H]<sup>+</sup> and 161.01 [Glc + H]<sup>+</sup>, compound 9 was verified as kaempferol-3-*O*-glucoside. *p*-Coumaric acid (Compound 10) was easily identified by comparison of mass spectrometry, standard and the database ([Wang et al., 2018a](#)). Compound 11 indicating the parent ion [C<sub>15</sub>H<sub>10</sub>O<sub>7</sub> + H]<sup>+</sup> at 303.05, was assigned as quercetin. Compound 12 with quasimolecular [M–H]<sup>-</sup> ion at 271.07 was identified as naringenin ([Wang et al., 2021](#)). Additionally, compound 13 showing the molecular ion at 287.02

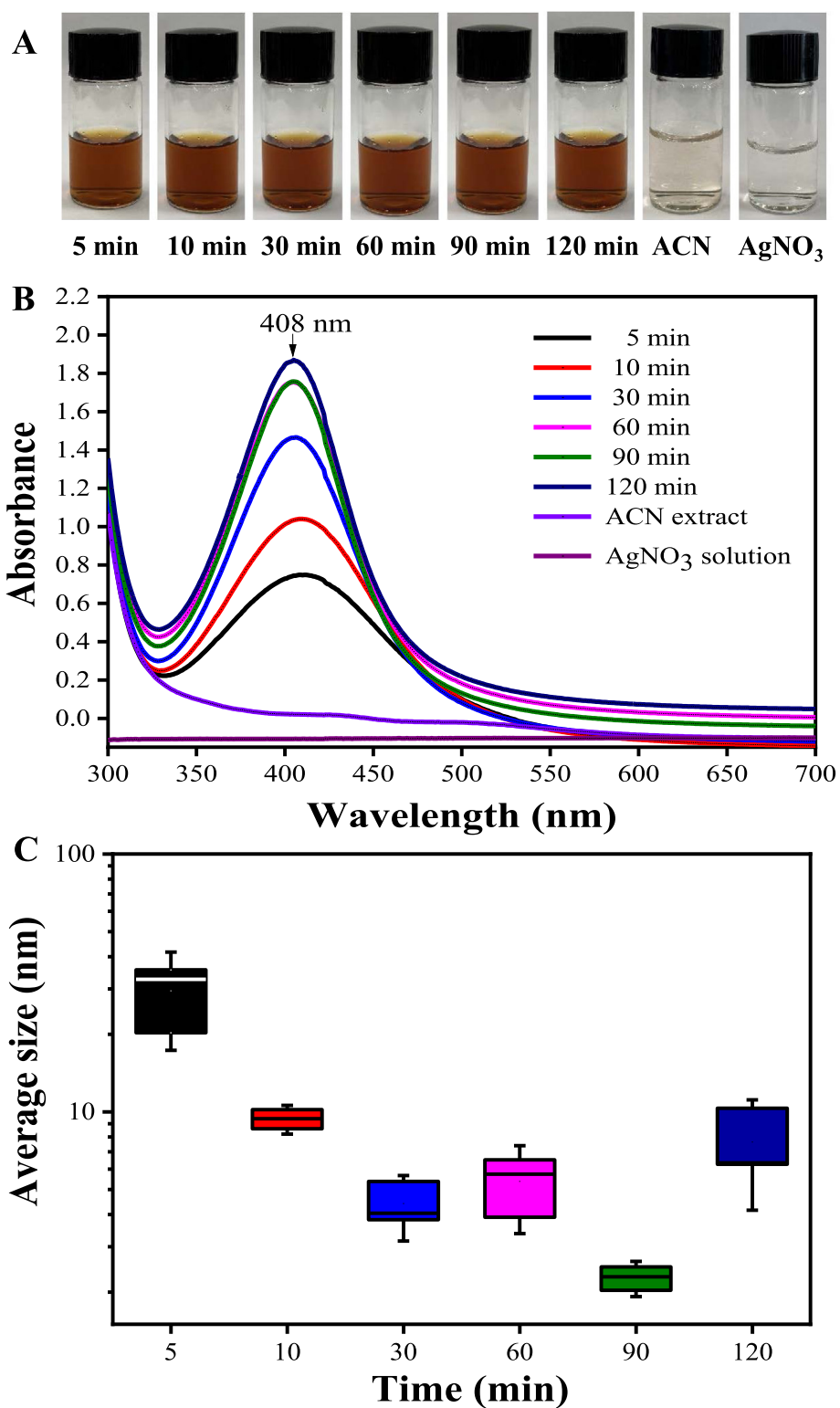


**Fig. 4** The color (A), UV-vis spectra (B) and the average size (C) changes of the bio-reduction kinetics of a colloidal AgNPs solution synthesized by the ACN aqueous extracts (1 mg/mL) and AgNO<sub>3</sub> (1.0 mM) under different reaction times at pH = 12.0, 25 °C.

[C<sub>15</sub>H<sub>10</sub>O<sub>6</sub> + H]<sup>+</sup> was easily determined as kaempferol. Many studies have confirmed that gallic acid, catechins derivatives, kaempferol, quercetin, and naringenin from plant extracts can be widely used as natural antioxidants in food and

medicinal industries (Hajipour et al., 2012; Wu et al., 2021). These natural antioxidants have health-promoting functions, such as preventing oxidative damage, reducing the blood sugar, and diminishing inflammation. In addition, these active

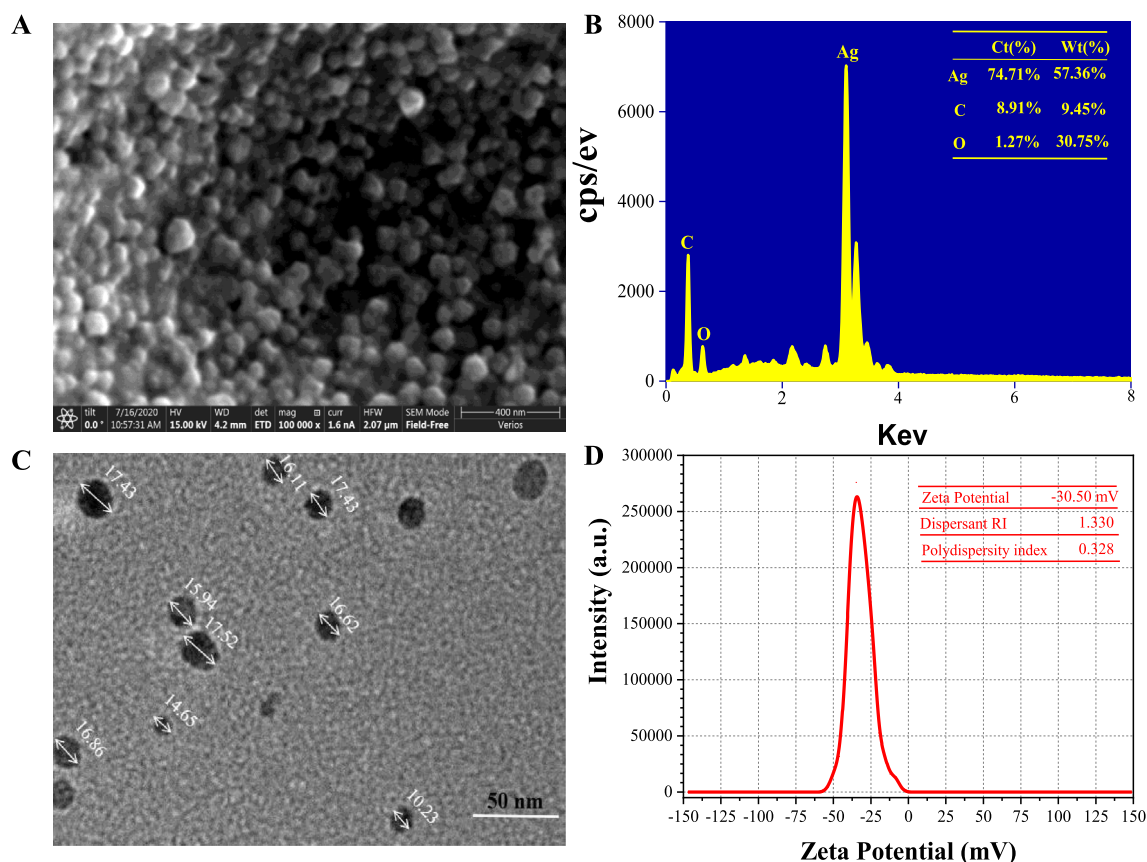


**Fig. 5** SEM image (100,000×) (A), EDX spectrum (B), TEM image (C) and Zeta potential value (C) of the purified AgNPs synthesized under the optimal synthesis parameters (pH value at 12.0 of the extract; 1.0 mM of AgNO<sub>3</sub> concentration; 90 min of reaction time).

secondary metabolites such as phenolics, flavonoids and enzymes from plant extracts can also be used as the reductants in synthesis of nanoparticles (Begic et al., 2021; Lotfollahzadeh et al., 2021). In this work, LC-MS identification of the chemical components of ACN aqueous extract was carried out to explain the active molecular mechanism for the synthesis of AgNPs (Fig. S1).

### 3.4. Antioxidant activity of the synthesized AgNPs

In this work, the antioxidant activities of as-prepared AgNPs were evaluated using DPPH<sup>•</sup> and ABTS<sup>•+</sup> assays. As shown in Fig. 8AB, regardless of DPPH<sup>•</sup> or ABTS<sup>•+</sup> assays, it was found that the radical scavenging activities of the AgNPs increased with the concentration of nanoparticles. It was observed that the DPPH<sup>•</sup> and ABTS<sup>•+</sup> radical scavenging activities reached 56.23% and 60.10% at 50 μg/mL Vc, respectively. However, the DPPH<sup>•</sup> radical scavenging activity reached 71.07% at 20 μg/mL AgNPs. The ABTS<sup>•+</sup> radical scavenging activity reached 76.70% at 50 μg/mL AgNPs. When the concentration of AgNPs was 100 μg/mL, the radical scavenging activities of DPPH<sup>•</sup> and ABTS<sup>•+</sup> were 87.40% and 87.47%, respectively. No significant differences in DPPH<sup>•</sup> and ABTS<sup>•+</sup> radical scavenging activities were observed between the synthesized AgNPs and Vc at the concentration over 100 μg/mL (Fig. 8AB). Wang et al. (2018a,b) reported that

the DPPH<sup>•</sup> radical scavenging activity reached 45.13% when tested with 100 μg/mL AgNPs synthesized using *Psidium guava* L. leaves extract, which was lower than the results of our study (87.40%). The results indicated that the synthesized AgNPs had excellent antioxidant activities (DPPH<sup>•</sup>, IC<sub>50</sub> = 11.75 ± 0.29 μg/mL; ABTS<sup>•+</sup>, IC<sub>50</sub> = 44.85 ± 0.37 μg/mL), and higher DPPH<sup>•</sup> and ABTS<sup>•+</sup> radical scavenging activities than of Vc (DPPH<sup>•</sup>, IC<sub>50</sub> = 58.64 ± 1.21 μg/mL; ABTS<sup>•+</sup>, IC<sub>50</sub> = 51.55 ± 0.31 μg/mL). Nwude Eze and Nwabor (2020) verified that the AgNPs synthesized with *Pichia* spent medium had potent free radical scavenging activities. As shown in FTIR, high antioxidant activities of AgNPs might be due to the presence of different types of active molecules (phenolics, flavonoids, sugar and etc.) distributed on the surfaces of AgNPs. Many researchers have confirmed these active compounds not only play important roles in the bio-reduction of Ag ions into AgNPs, but also can scavenge the free radical species by the donation of electrons or hydrogen atoms from the active molecules distributed on the surfaces of AgNPs (Kup et al., 2020; Yousaf et al., 2020).

### 3.5. Antibacterial activity of AgNPs

To investigate the application potential of AgNPs as an antibacterial agent, the MIC and MBC of the synthesized AgNPs, AgNO<sub>3</sub> solution and the ACN aqueous extract were

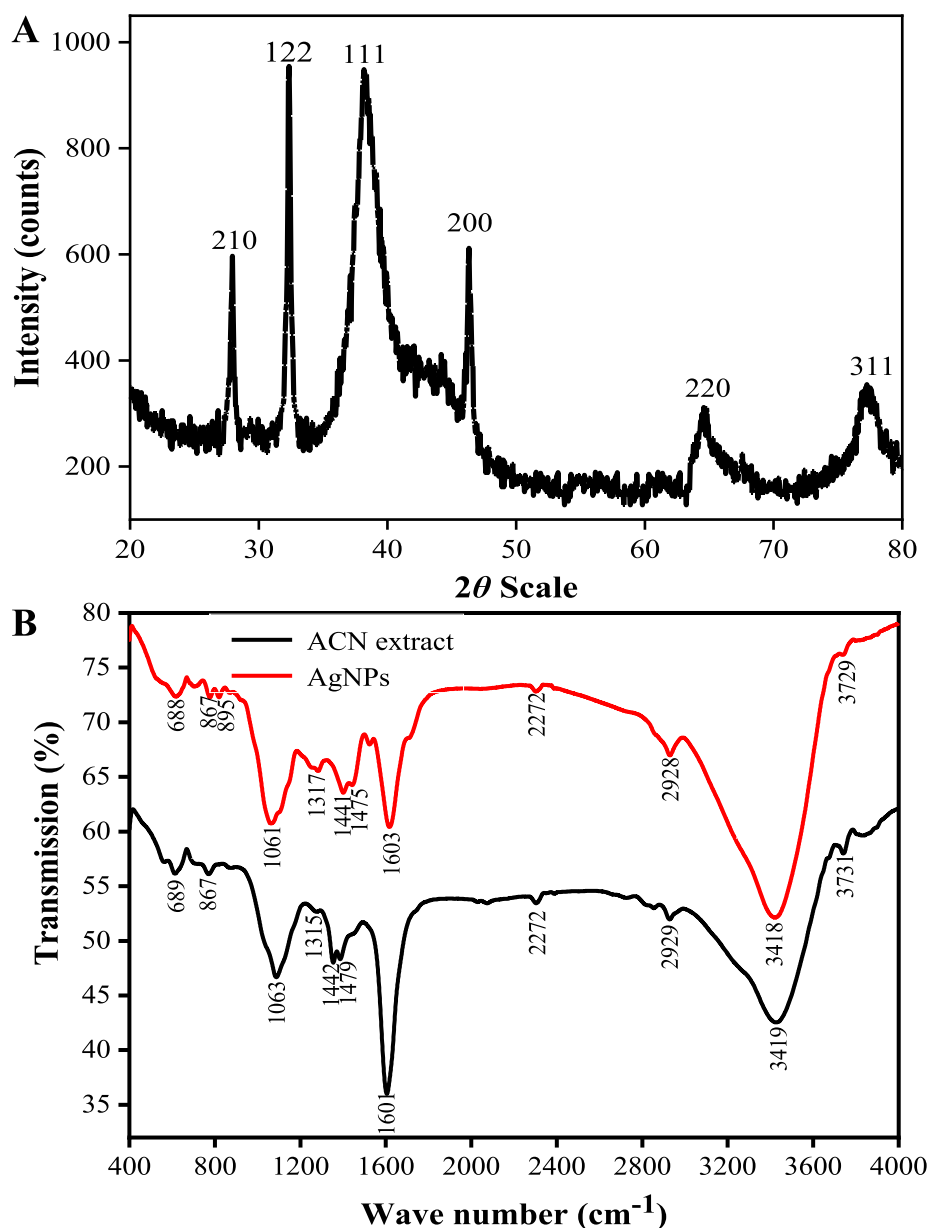


**Fig. 6** XRD pattern (A) and FTIR analysis (B) of the synthesized AgNPs under the optimal conditions (pH value at 12.0 of the extract; 1.0 mM of  $\text{AgNO}_3$  concentration; 90 min of reaction time).

evaluated by six common foodborne pathogens. As shown in Table 2, the ACN aqueous extracts exhibited significant inhibitory effects on all investigated bacteria (MIC: 64–512  $\mu\text{g}/\text{mL}$ ; MBC: 128–1024  $\mu\text{g}/\text{mL}$ ), especially *S. typhimurium* (MIC = 64  $\mu\text{g}/\text{mL}$ ; MBC = 128  $\mu\text{g}/\text{mL}$ ).  $\text{AgNO}_3$  solution (MIC ranging from 32 to 256  $\mu\text{g}/\text{mL}$ ; MBC ranging from 32 to 256  $\mu\text{g}/\text{mL}$ ) exhibited more stronger anti-bacterial activities against all investigated bacteria than the ACN aqueous extracts (MIC: 64–512  $\mu\text{g}/\text{mL}$ ; MBC: 128–1024  $\mu\text{g}/\text{mL}$ ). AgNPs exhibited even stronger anti-bacterial activities against *S. aureus* (MIC = 4  $\mu\text{g}/\text{mL}$ ; MBC = 8  $\mu\text{g}/\text{mL}$ ) and *E. coli* (MIC = 4  $\mu\text{g}/\text{mL}$ ; MBC = 8  $\mu\text{g}/\text{mL}$ ). Moreover, the antibiotics Tetracycline Hydrochloride showed the strongest anti-bacterial activities against all investigated bacteria (MIC: 1–4  $\mu\text{g}/\text{mL}$ ; MBC:

2–8  $\mu\text{g}/\text{mL}$ ), especially *E. coli* (MIC = 1  $\mu\text{g}/\text{mL}$ ; MBC = 2  $\mu\text{g}/\text{mL}$ ) and *S. aureus* (MIC = 2  $\mu\text{g}/\text{mL}$ ; MBC = 2  $\mu\text{g}/\text{mL}$ ). It was observed that Gram positive bacteria were significantly more susceptible to all antibacterial agents compared with Gram negative bacteria. Researchers have verified that Gram positive bacteria were not evidently more sensitive to AgNPs than Gram negative bacteria (Baygar et al., 2019; Mahmoudi et al., 2019ab; Wang et al., 2018b). Due to the structural differences of cell wall, AgNPs can more easily enter the cell membrane or cytoplasm, and interact with proteins/enzymes/DNA of Gram negative bacteria, and ultimately cause apoptosis (Álvarez-Chimal et al., 2021; Huang et al., 2020). Similar results were reported from Ramanathan et al., who found that eco-friendly synthesized *S. trilobatum* extract-capped AgNPs

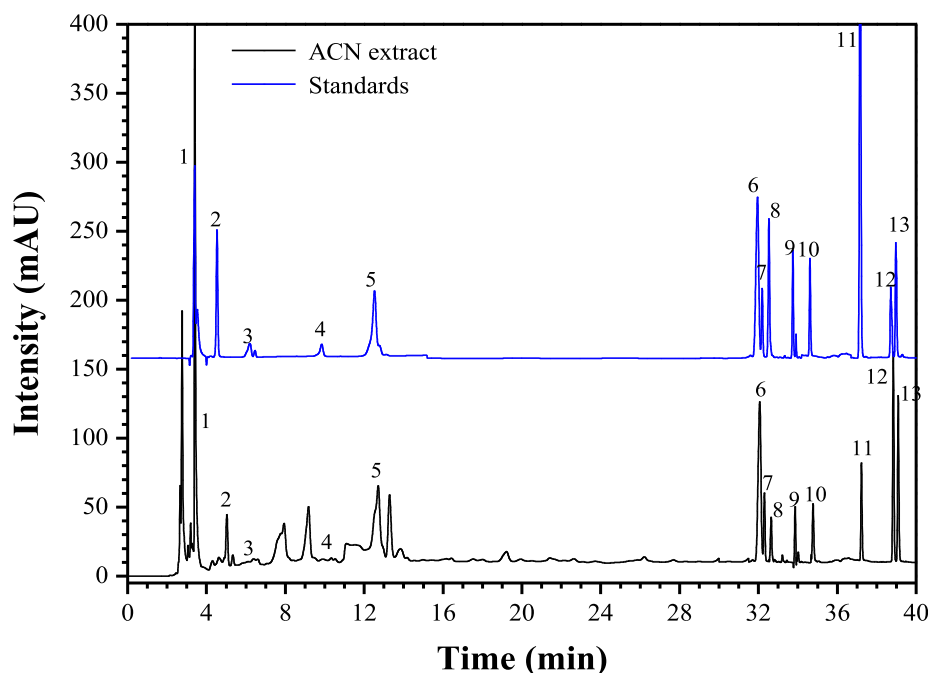


**Fig. 7** HPLC chromatograms of chemical compositions in the ACN aqueous extracts and the standards. 1, gallic acid; 2, (–)-gallocatechin; 3, (–)-epigallocatechin; 4, d-catechin; 6, ferulic acid; 7, rutin; 8, quercetin-3-*O*-galactoside; 9, kaempferol-3-*O*-glucoside; 10, *p*-coumaric acid; 11, quercetin; 12, naringenin; 13, kaempferol.

**Table 1** Identification of the main chemical constituents of ACN aqueous extract by HPLC-ESI-qTOF-MS/MS.

Peak No.	RT (min)	$\lambda_{\max}$ (nm)	Molecular ion ( $m/z$ )	MS/MS ( $m/z$ )	Mw	Formula	Compounds	Error	Reference
1	3.25	245, 278	171.02 [M+H] <sup>+</sup>	171.02, 127.02	170	C <sub>7</sub> H <sub>6</sub> O <sub>5</sub>	Gallic acid	0.28	Standard, MS/MS
2	4.92	254, 350	307.08[M+H] <sup>+</sup>	306.08, 139.01	306	C <sub>15</sub> H <sub>14</sub> O <sub>7</sub>	(–)-Gallocatechin	–1.23	Standard, MS/MS
3	6.03	256, 354	307.07[M+H] <sup>+</sup>	306.07, 139.01	306	C <sub>15</sub> H <sub>14</sub> O <sub>7</sub>	Epigallocatechin	0.95	Standard, MS/MS
4	9.18	260, 283	291.07 [M+H] <sup>+</sup>	291.07	290	C <sub>15</sub> H <sub>14</sub> O <sub>6</sub>	D-catechin	3.10	Standard, MS/MS
5	12.28	254, 350	256.07[M+H] <sup>+</sup>	256.073	257	C <sub>15</sub> H <sub>12</sub> O <sub>4</sub>	Unknown	–0.72	–
6	32.01	261, 280	193.05 [M+H] <sup>+</sup>	178.03, 134.04	194	C <sub>10</sub> H <sub>10</sub> O <sub>4</sub>	Ferulic acid	–0.93	Standard, MS/MS
7	32.15	254, 352	609.15[M+H] <sup>+</sup>	609.15, 463.50, 301.03, 161.21	610	C <sub>27</sub> H <sub>30</sub> O <sub>16</sub>	Rutin	2.53	Standard, MS/MS
8	32.63	257, 372	593.16 [M+H] <sup>+</sup>	593.16, 433.21, 303.16, 153.03	594	C <sub>27</sub> H <sub>30</sub> O <sub>15</sub>	Quercetin-3- <i>O</i> -galactoside	2.17	Standard, MS/MS
9	33.95	254, 350	449.11 [M+H] <sup>+</sup>	449.11, 287.06	448	C <sub>21</sub> H <sub>20</sub> O <sub>11</sub>	Kaempferol-3- <i>O</i> -glucoside	1.90	Standard, MS/MS
10	34.87	254, 280	165.05 [M+H] <sup>+</sup>	165.05, 119.05	164	C <sub>9</sub> H <sub>8</sub> O <sub>3</sub>	<i>p</i> -Coumaric acid	–1.43	Standard, MS/MS
11	37.21	280, 367	303.07[M+H] <sup>+</sup>	303.07, 137.62	303	C <sub>15</sub> H <sub>10</sub> O <sub>7</sub>	Quercetin	–2.16	Standard, MS/MS
12	38.92	257, 350	271.07 [M+H] <sup>+</sup>	271.07, 151.08	272	C <sub>15</sub> H <sub>12</sub> O <sub>5</sub>	Naringenin	1.13	Standard, MS/MS
13	39.07	254, 364	287.27 [M+H] <sup>+</sup>	287.27	286	C <sub>15</sub> H <sub>10</sub> O <sub>6</sub>	Kaempferol	0.76	Standard, MS/MS

had enhanced antimicrobial properties. Wang et al. (2018a) reported that the AgNPs prepared with the aqueous extract of guava leaf exhibited much higher anti-microbial activity than AgNPs synthesized with other materials. With regard to the antibacterial mechanism of AgNPs, no consensus has been reported yet. Pal et al. (2007) reported that the synthesized AgNPs can easily cross the bacteria cell wall and destroy

the cells due to their spherical morphology and the small size. It is obvious that the binding of nanoparticles to the microorganism depends on the surface area available for interaction. Compared with big-sized nanoparticles, smaller-sized silver nanoparticles have a larger surface area for interaction with microorganism, and thus have a stronger antibacterial activity. Extensive studies have also suggested that ROS

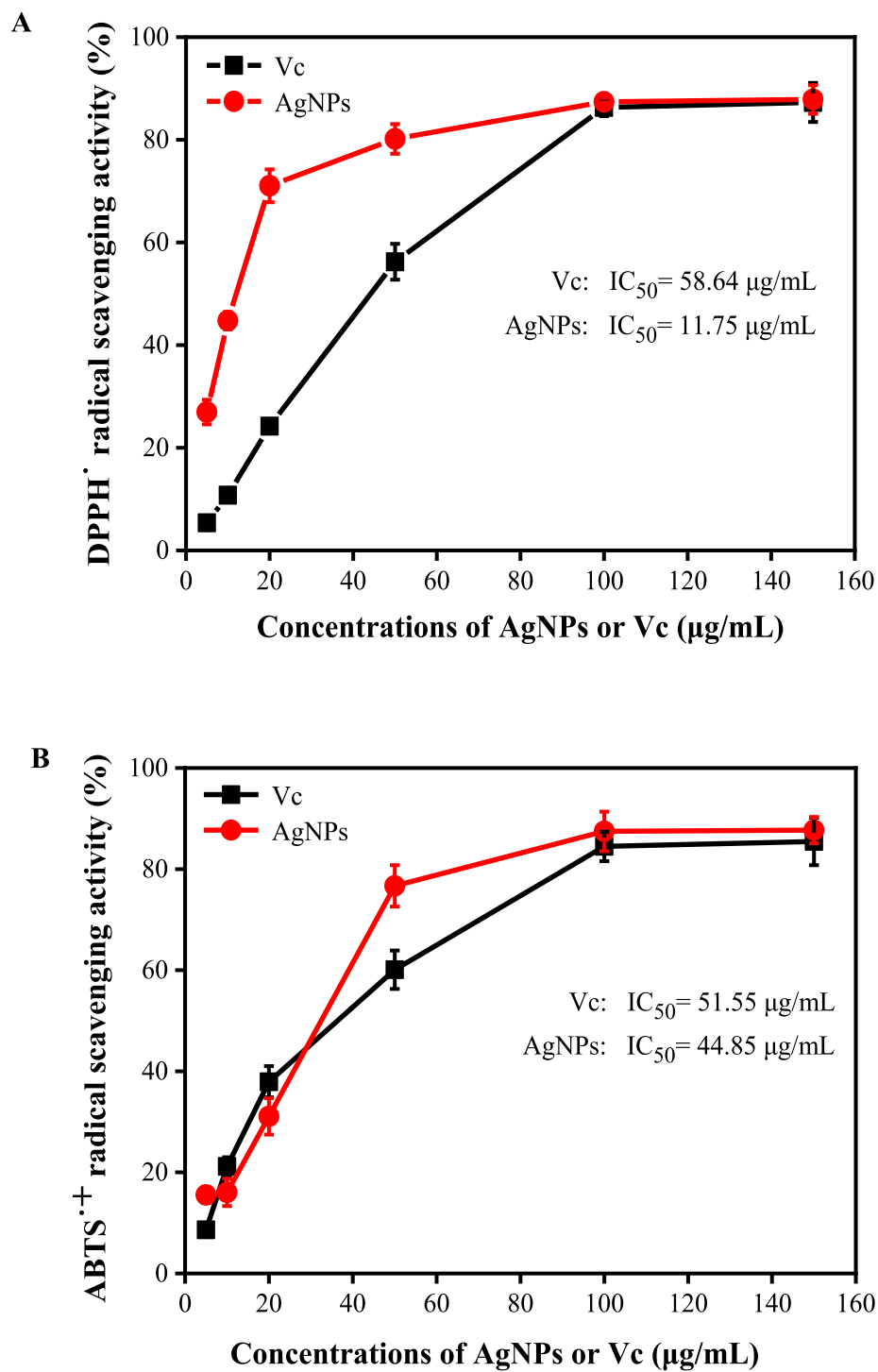


**Fig. 8** The radical scavenging activities of DPPH (A) and ABTS $\cdot^+$  (B) of AgNPs synthesized by the ACN aqueous extract and AgNO $_3$  solution under the optimal conditions.

**Table 2** Anti-bacterial activities (MIC and MBC) of AgNPs, the ACN aqueous extract, AgNO<sub>3</sub> solution and Tetracycline Hydrochloride.

Strains	MIC (µg/mL)				MBC (µg/mL)			
	AgNPs	Tetracycline Hydrochloride	Extract	AgNO <sub>3</sub>	AgNPs	Tetracycline Hydrochloride	Extract	AgNO <sub>3</sub>
<b>Gram negative bacteria</b>								
<i>Escherichia coli</i>	4	1	256	32	8	2	256	32
<i>Salmonella typhimurium</i>	8	2	64	32	8	4	128	64
<i>Pseudomonas aeruginosa</i>	8	4	256	32	16	4	512	64
<b>Gram positive bacteria</b>								
<i>Listeria monocytogenes</i>	16	4	512	64	32	8	512	128
<i>Staphylococcus aureus</i>	4	2	512	64	8	2	–	128
<i>Bacillus subtilis</i>	16	4	256	256	64	8	1024	256

generated in the cell is considered as a key mechanism, which accounts for the antimicrobial potential of AgNPs. ROS led to cellular membranes disrupting, proteins/enzymes denaturation, and DNA damage, resulting in cell death (Aguirre et al., 2020; Kup et al., 2020).

#### 4. Conclusions

In this work, stable and nearly spherical silver nanoparticles were synthesized by using the aqueous extracts of *A. catechu* L. nut as a reducing and capping agent. The size of AgNPs was sensitive to the synthesis parameters. Under the extract pH value of 12.0, AgNO<sub>3</sub> concentration of 1.0 mM, and reaction time of 90 min, the synthesized AgNPs were stable and well-dispersed, and in regular spherical shape, with average particle size of 15–20 nm. Also, the formation of AgNPs using the ACN aqueous extract was confirmed by using UV–Vis, XRD, SEM, TEM and FTIR techniques. Additionally, the possible reductants in the aqueous extract of ACN were identified, which accounted for the possible mechanism for the reduction of Ag<sup>+</sup> ion. Importantly, the synthesized AgNPs were effective in the scavenging of free radical. AgNPs showed an improved anti-bacterial activities against six tested foodborne pathogens. In conclusion, the size-controlled AgNPs synthesized by using the ACN aqueous extract can be used as a promising anti-oxidant and anti-bacterial agent.

#### CRedit authorship contribution statement

**Xiaoping Hu:** Methodology, Investigation, Data curation.  
**Lingfeng Wu:** Methodology, Investigation, Data curation.  
**Minjie Du:** Data curation, Writing – review & editing. **Lu Wang:** Supervision, Data curation, Writing – review & editing.

#### Declaration of Competing Interest

The authors declare that they have no known competing financial interests or personal relationships that could have appeared to influence the work reported in this paper.

#### Acknowledgments

This work was supported by the Scientific Research Foundation of Hainan University (No. KYQD(ZR)1901) and the Natural Science Foundation of Hainan Province (No. 2019RC009).

#### Appendix A. Supplementary material

Supplementary data to this article can be found online at <https://doi.org/10.1016/j.arabjc.2022.103763>.

#### References

- Ahmad, F., Muhammad Taj, B., Ramzan, M., Ali, H., Ali, A., Adeel, M., Iqbal, M.N., Imran, M., 2021. One-pot synthesis and characterization of in-house engineered silver nanoparticles from *Flacourtia jangomas* fruit extract with effective antibacterial profiles. *J. Nanostruct. Chem.* 11 (3), 131–141.
- Álvarez-Chimal, R., García-Pérez, V.I., Álvarez-Pérez, M.A., Arenas-Alatorre, J.Á., 2021. Green synthesis of ZnO nanoparticles using a *Dysphania ambrosioides* extract: Structural characterization and antibacterial properties. *Mater. Sci. Eng. C* 118, 111540.
- Ameen, F., Dawoud, T., AlNadhari, S., 2021. Ecofriendly and low-cost synthesis of ZnO nanoparticles from *Acremonium potronii* for the photocatalytic degradation of azo dyes. *J. Environ. Manage.* 202, 111700.
- Aguirre, D.P.R., Loyola, E.F., Salcido, N.M.D.L.F., Sifuentes, L.R., Moreno, A.R., Jolas, J.E.M., 2020. Comparative antibacterial potential of silver nanoparticles prepared via chemical and biological synthesis. *Arab. J. Chem.* 13, 8662–8670.
- Aygün, A., Gülbağça, F., Nas, M.S., Alma, M.H., Şen, F., 2020. Biological synthesis of silver nanoparticles using *Rheum ribes* and evaluation of their anticarcinogenic and antimicrobial potential: A novel approach in phytonanotechnology. *J. Pharma. Biomed. Anal.* 179, 113012.
- Baygar, T., Sarac, N., Ugur, A., Karac, I.R., 2019. Antimicrobial characteristics and biocompatibility of the surgical sutures coated with biosynthesized silver nanoparticles. *Bioorg. Chem.* 86, 254–258.
- Begic, N., Bener, M., Apak, R., 2021. Development of a green synthesized silver nanoparticle-based antioxidant capacity method using carob extract. *J. Nanostruct. Chem.* <https://doi.org/10.1007/s40097-020-00374-6>.
- Bejene, H.D., Werkneh, A.A., Bezabh, H.K., Ambaye, T.G., 2017. Synthesis paradigm and applications of silver nanoparticles (Ag NPs), a review. *Sus. Mater. Technol.* 13, 18–23.
- Bhat, R., Ganachari, S.V., Deshpande, R., Ravindra, G., 2012. Venkataraman, A.: Rapid biosynthesis of silver nanoparticles using *Areca nut (Areca catechu)* extract under microwave-assistance. *J. Clust. Sci.* 24, 107–114.
- Ebrahimzadeha, M.A., Naghizadeh, A., Amiric, O., Shirzadi-Ahondashti, M., Mortazavi-Derazkol, S., 2020. Green and facile synthesis of Ag nanoparticles using *Crataegus pentagyna* fruit

- extract (CP-AgNPs) for organic pollution dyes degradation and antibacterial application. *Bioorg. Chem.* 94, 103425.
- Gur, T., Meydan, I., Seckin, H., Bekmezci, M., Sen, F., 2022. Green synthesis, characterization and bioactivity of biogenic zinc oxide nanoparticles. *Environ. Res.* 204, 111897.
- Hajipour, M.J., Fromm, K.M., Shkarran, A.A., Aberasturi, D.J., Larramendi, I.R., Serpooshan, T.R., Parak, W.J., Mahmoudi, M., 2012. Antibacterial properties of nanoparticle. *Trends Biotechnol.* 10, 499–511.
- Huang, H., Shan, K.Z., Liu, J.B., 2020. Synthesis, optimization and characterization of silver nanoparticles using the catkin extract of *Piper longum* for bactericidal effect against food-borne pathogens via conventional and mathematical approaches. *Bioorg. Chem.* 103, 104230.
- Iravani, S., 2011. Green synthesis of metal nanoparticles using plants. *Green Chem.* 13, 2638–2650.
- Jorgensen, J.H., 1993. NCCLS methods for dilution antimicrobial susceptibility tests for bacteria that grow aerobically, approved standard. *Infect. Dis. Clin. N. AM.* 7, 393–409.
- Kanagamani, K., Muthukrishnan, P., Shankar, K., Kathiresan, A., Barabadi, H., Saravanan, M., 2019. Antimicrobial, cytotoxicity and photocatalytic degradation of norfloxacin using *Kleintia grandiflora* mediated silver nanoparticles. *J. Clust. Sci.*, 1415–1424
- Kup, F.O., Coskuncay, S., Duman, F., 2020. Biosynthesis of silver nanoparticles using leaf extract of *Aesculus hippocastanum* (horse chestnut): evaluation of their antibacterial, antioxidant and drug release system activities. *Mater. Sci. Eng. C.* 107, 110207.
- Kuznetsova, Y.V., Rempela, A.A., 2015. Size and zeta potential of Cds nanoparticles in stable aqueous solution of EDTA and NaCl. *Inorg. Mater.* 51, 215–219.
- Lee, S.H., Jun, B.H., 2019. Silver nanoparticles: synthesis and application for nanomedicine. *Int. J. Mol. Sci.* 20, 24.
- Li, S.J., Wang, R.M., Hu, X.P., Li, C.F., Wang, L., 2022. Bio-affinity ultra-filtration combined with HPLC-ESI-qTOF-MS/MS for screening potential  $\alpha$ -glucosidase inhibitors from *Cerasus humilis* (Bge.) Sok. leaf-tea and in silico analysis. *Food Chem.* 373, 131528.
- Lin, X., Wu, L.F., Wang, X., Yao, L.L., Wang, L., 2021. Ultrasonic-assisted extraction for flavonoid compounds content and antioxidant activities of India *Moringa oleifera* L. leaves: simultaneous optimization, HPLC characterization and comparison with other methods. *J. Appl. Res. Med. Aroma.* 20, 100284.
- Lotfollahzadeh, R., Yari, M., Sedaghat, S., Delbari, A.S., 2021. Biosynthesis and characterization of silver nanoparticles for the removal of amoxicillin from aqueous solutions using *Oenothera biennis* water extract. *J. Nanostruct. Chem.* <https://doi.org/10.1007/s40097-021-00393-x>.
- Mahmoudi, R., Aghaei, S., Salehpour, Z., Mousavizadeh, A., Bardania, H., 2019a. Antibacterial and antioxidant properties of phyto-synthesized silver nanoparticles using *Lavandula stoechas* extract. *Appl. Organomet. Chem.* 34, (2) e5394.
- Mahmoudi, R., Ardakani, M.T., Verdom, B.H., Bagheri, A., Mohammad-Beigi, H., Aliakbari, F., et al. 2019b. Chitosan nanoparticles containing *Physalis alkekengi* L. extract: preparation, optimization and their antioxidant activity. *B. Mater. Sci.* 42 (3), 1–6.
- Mani, M., Harikrishnan, R., Purushothaman, P., Pavithra, S., Rajkumar, P., Kumaresan, S., Al Farraj, D.A., Elshikh, M.S., Balasubramanian, B., Kaviyarasu, K., 2021a. Systematic green synthesis of silver oxide nanoparticles for antimicrobial activity. *Environ. Res.* 202, 111627.
- Mani, M., Pavithra, S., Mohanraj, K., Kumaresan, S., Alotaibi, S.S., Eraqi, M.M., Gandhi, A.D., Babujanathanam, R., Maaza, M., Kaviyarasu, K., 2021b. Studies on the spectrometric analysis of metallic silver nanoparticles (AgNPs) using *Basella alba* leaf for the antibacterial activities. *Environ. Res.* 199, 111274.
- Mani, M., Mohammad, K.O., Selvaraj, S., Ram Kumar, A., Kumaresan, S., Muthukumar, A., Kaviyarasu, K., El-Tayeb, M.A., Elbadawi, Y.B., Almaary, K.S., Almunqedhi, B.M.A., Elshikh, M.S., 2021c. A novel biogenic *Allium cepa* leaf mediated silver nanoparticles for antimicrobial, antioxidant, and anticancer effects on MCF-7 cell line. *Environ. Res.* 202, 111199.
- Momeni, S.S., Nasrollahzadeh, M., Rustaiyan, A., 2017. Biosynthesis and application of Ag/bone nanocomposite for the hydration of cyanamides in *Myrica gale* L. extract as a green solvent. *J. Colloid. Interface. Sci.* 499, 93–101.
- Nwude Eze, F., Nwabor, O.F., 2020. Valorization of *Pichia spent* medium via one-pot synthesis of biocompatible silver nanoparticles with potent antioxidant, antimicrobial, tyrosinase inhibitory and reusable catalytic activities. *Mater. Sci. Eng. C.* 115, 111104.
- Pal, S., Yu, K.T., Song, J.M., 2007. Does the antibacterial activity of silver nanoparticles depend on the shape of the nano-particle? a study of the gram-negative bacterium *Escherichia coli*. *Appl. Environ. Microb.* 73 (6), 1712–1720.
- Prema, P., Veeramankandan, V., Rameshkumar, K., Gatasheh, M.K., Hatamleh, A.A., Balasubramani, R., Balaji, P., 2022. Statistical optimization of silver nanoparticle synthesis by green tea extract and its efficacy on colorimetric detection of mercury from industrial waste water. *Environ. Res.* 204, 111915.
- Rajan, A., Vilas, V., Philip, D., 2015. Catalytic and antioxidant properties of biogenic silver nanoparticles synthesized using *Areca catechu* nut. *J. Mol. Liq.* 207, 231–236.
- Rasheed, T., Shafi, S., Bilal, M., Hussain, T., Sher, F., Rizwan, K., 2020a. Surfactants-based remediation as an effective approach for removal of environmental pollutants-a review. *J. Mol. Liq.* 318, 113960.
- Rasheed, T., Ahmad, N., Nawaz, S., Sher, F., 2020b. Photocatalytic and adsorptive remediation of hazardous environmental pollutants by hybrid nanocomposites. *Case Studies. Chem. Environ. Eng.* 2, 100037.
- Sathishkumar, M., Sneha, K., Won, S.W., Cho, C.W., Kim, S., Yun, Y.S., 2009. *Cinnamon zeylanicum* bark extract and powder mediated green synthesis of nano-crystalline silver particles and its bactericidal activity. *Colloids Surf. B* 73, 332–338.
- Sazwi, N.N., Nalina, T., Rahim, Z.H.A., 2013. Antioxidant and cytoprotective activities of *Piper betle*, *Areca catechu*, *Uncaria gambir* and *Betel quid* with and without calcium hydroxide. *BMC Complem. Altern. M.* 13, 351.
- Sher, F., Hanif, K., Rafey, A., Khalid, U., Lima, E.C., 2020. Removal of micropollutants from municipal wastewater using different types of activated carbons. *J. Environ. Manage.* 278, (2) 111302.
- Shen, X., Chen, W., Zheng, Y., Lei, X., Tang, M., Wang, H., 2017. Chemical composition, antibacterial and antioxidant activities of hydrosols from different parts of *Areca catechu* L. and *Cocos nucifera* L. *Ind. Crops. Prod.* 96, 110–119.
- Verma, A., Mehata, M.S., 2020. Controllable synthesis of silver nanoparticles using *Neem* leaves and their antimicrobial activity. *J. Radiat. Res. Appl. Sci.* 9, 109–115.
- Venkataadri, B., Shanparvish, E., Rameshkumar, M.R., Arasu, M.V., Al-Dhabi, N.A., Ponnusamy, V.K., Agastian, P., 2020. Green synthesis of silver nanoparticles using aqueous rhizome extract of *Zingiber officinale* and *Curcuma longa*: In-vitro anti-cancer potential on human colon carcinoma HT-29 cells. *Saudi J. Biol. Sci.* 27, 2980–2986.
- Wang, L., Lu, F.J., Liu, Y., Wu, Y.N., Wu, Z.Q., 2018a. Photocatalytic degradation of organic dyes and antimicrobial activity of silver nanoparticles fast synthesized by flavonoids fraction of *Psidium guajava* L. leaves. *J. Mol. Liq.* 263, 187–192.
- Wang, L., Wu, Y.N., Xie, J., Wu, S., Wu, Z.Q., 2018b. Characterization, antioxidant and antimicrobial activities of green synthesized silver nanoparticles from *Psidium guajava* L. leaf aqueous extracts. *Mater. Sci. Eng. C.* 86, 1–8.
- Wang, R.M., Pan, F.B., He, R.P., Kuang, F.J., Wang, L., Lin, X., 2021. Arecanut (*Areca catechu* L.) seed extracts extracted by conventional and eco-friendly solvents: Relation between phytochemical compositions and biological activities by multivariate analysis. *J. Appl. Res. Med. Aroma.* 25, 100336.

- Wang, R.M., Yao, L.L., Lin, X., Hu, X.P., Wang, L., 2022. Exploring the potential mechanism of *Rhodomyrtus tomentosa* (Ait.) Hassk fruit phenolic rich extract on ameliorating nonalcoholic fatty liver disease by integration of transcriptomics and metabolomics profiling. *Food. Res. Int.* 151, 110824.
- Wei, S.M., Wang, Y.H., Tang, Z.S., Hu, J.H., Su, R., Lin, J.J., Zhou, T., Guo, H., Wang, N., Xu, R.R., 2020. A size-controlled green synthesis of silver nanoparticles by using the berry extract of *Sea Buckthorn* and their biological activities. *New J. Chem.* 44, 9304.
- Wei, S.M., Wang, Y.H., Tang, Z.S., Xu, H.B., Wang, Z., Yang, T., Zhou, T.Y., 2021. A novel green synthesis of silver nanoparticles by the residues of Chinese herbal medicine and their biological activities. *RSC Adv.* 11, 1411.
- Wu, L.F., Chen, Z.N., Li, S.J., Wang, L., Zhang, J.C., 2021. Eco-friendly and high-efficient extraction of natural antioxidants from *Polygonum aviculare* leaves using tailor-made deep eutectic solvents as extractants. *Sep. Purif. Technol.* 262, 118339.
- Wu, L.F., Li, L., Chen, S.J., Wang, L., Lin, X., 2020. Deep eutectic solvent-based ultrasonic-assisted extraction of phenolic compounds from *Moringa oleifera* L. leaves: Optimization, comparison and antioxidant activity. *Sep. Purif. Technol.* 247, 117014.
- Yousaf, H., Mehmood, A., Ahmad, K.S., Raffi, M., 2020. Green synthesis of silver nanoparticles and their applications as an alternative antibacterial and antioxidant agents. *Mater. Sci. Eng. C* 112, 110901.
- Yulizar, Y., Kusriani, E., Apriandanu, D.O.B., Nurdini, N., 2020. *Datura metel* L. leaves extract mediated CeO<sub>2</sub> nanoparticles: synthesis, characterizations, and degradation activity of DPPH radical. *Surf. Interfaces.* 19, 100437.
- Yuvakkumar, R., Suresh, J., Nathanael, A.J., Sundrarajan, M., Hong, S.I., 2014. Novel green synthetic strategy to prepare ZnO nanocrystals using rambutan (*Nephelium lappaceum* L.) peel extract and its antibacterial applications. *Mater. Sci. Eng. C* 41, 17–27.
- Zhu, H.L., Zhang, J.C., Li, C.F., Liu, S.X., Wang, L., 2020. *Morinda citrifolia* L. leaves extracts obtained by traditional and eco-friendly extraction solvents: Relation between phenolic compositions and biological properties by multivariate analysis. *Ind. Crops. Prod.* 153, 112586.